

Simultaneously Magnetic- and Electric-dipole Active Spin Excitations Govern the Static Magnetoelectric Effect in Multiferroic Materials

Dávid Szaller,¹ Sándor Bordács,² Vilmos Kocsis,¹ Toomas Rõõm,³ Urmas Nagel,³ and István Kézsmárki^{1,4}

¹*Department of Physics, Budapest University of Technology and Economics, 1111 Budapest, Hungary*

²*Quantum-Phase Electronics Center, Department of Applied Physics, The University of Tokyo, Tokyo 113-8656, Japan*

³*National Institute of Chemical Physics and Biophysics, Akadeemia tee 23, 12618 Tallinn, Estonia*

⁴*Condensed Matter Research Group of the Hungarian Academy of Sciences, 1111 Budapest, Hungary*

(Dated: January 15, 2014)

We derive a sum rule to demonstrate that the static magnetoelectric (ME) effect is governed by optical transitions that are simultaneously excited via the electric and magnetic components of light. By a systematic analysis of magnetic point groups, we show that the ME sum rule is applicable to a broad variety of non-centrosymmetric magnets including ME multiferroic compounds. Due to the dynamical ME effect, the optical excitations in these materials can exhibit directional dichroism, i.e. the absorption coefficient can be different for counter-propagating light beams. According to the ME sum rule, the magnitude of the linear ME effect of a material is mainly determined by the directional dichroism of its low-energy optical excitations. Application of the sum rule to the multiferroic $\text{Ba}_2\text{CoGe}_2\text{O}_7$, $\text{Sr}_2\text{CoSi}_2\text{O}_7$ and $\text{Ca}_2\text{CoSi}_2\text{O}_7$ shows that in these compounds the static ME effect is mostly governed by the directional dichroism of the spin-wave excitations in the GHz-THz spectral range. On this basis, we argue that the studies of directional dichroism and the application of ME sum rule can promote the synthesis of new materials with large static ME effect.

I. INTRODUCTION

Magnetoelectric (ME) multiferroics, where ferroelectricity coexists with (ferro)magnetism, represent the most extensively studied class of multiferroics.¹⁻⁶ A spectacular control of the ferroelectric polarization by magnetic field and manipulation of the magnetic order via electric field can be realized in most of these materials as a direct consequence of the coupling between spins and local electric dipoles. This offers a fundamentally new path for data storage by combining the best qualities of ferroelectric and magnetoresistive memories: fast low-power electrical write operation, and non-destructive non-volatile magnetic read operation.^{5,6} The efficiency of multiferroics in such memory applications depends on the strength of the magnetization-polarization coupling responsible for the ME phenomena.

The ME effect has also been proposed to open new perspectives in photonics. The entanglement between spins and local polarization governs not only the ground-state properties but also the character of excited states. Consequently, the electric component of light can induce precession of the spins and the magnetic component of light can generate electric polarization waves. This is termed as the optical ME effect and has recently been observed for the spin excitations in several multiferroic compounds.⁷⁻¹⁵

As one of the most peculiar manifestations of the ME effect in the optical regime, counter-propagating light beams can experience different refractive indices in multiferroics. Strong directional dichroism, that is difference in the absorption coefficient for light beams traveling in opposite directions, has been reported for spin excitations in these materials and proposed as a new principle to design directional light switches operating in the GHz-THz region.¹⁰⁻¹⁴

Here, we show that optical studies of low energy magnons and phonons in ME multiferroics, provide an efficient tool to further elucidate microscopic mechanisms of multiferroicity.

These studies can be particularly useful to promote the systematic synthesis of new materials with large static ME effect. We derive a relation, hereafter referred to as the *ME sum rule*, which shows the connection between the static ME effect and the directional dichroism observed for low-energy excitations. We specify the class of materials where this ME sum rule is directly applicable. Finally, we investigate the consequences of the ME sum rule for three multiferroic materials, $\text{Ba}_2\text{CoGe}_2\text{O}_7$ (BCGO), $\text{Sr}_2\text{CoSi}_2\text{O}_7$ (SCSO) and $\text{Ca}_2\text{CoSi}_2\text{O}_7$ (CCSO). For this purpose, we compare their directional dichroism spectra to the corresponding static ME coefficients reported in the literature.¹⁶⁻²¹ Absorption measurements used to determine the directional dichroism in the GHz-THz spectral range were performed in the present study and partly reproduced from our former works.¹⁰⁻¹²

The Kramers-Kronig relation, also known as the Hilbert transformation, connects the real (\Re) and imaginary (\Im) parts of a general frequency dependent response function (susceptibility), $\chi(\omega)$, which corresponds to a linear and causal response function in the time domain:

$$\begin{aligned}\Re\chi(\omega) &= \frac{1}{\pi}\mathcal{P}\int_{-\infty}^{\infty}\frac{\Im\chi(\omega')}{\omega'-\omega}d\omega', \\ \Im\chi(\omega) &= -\frac{1}{\pi}\mathcal{P}\int_{-\infty}^{\infty}\frac{\Re\chi(\omega')}{\omega'-\omega}d\omega',\end{aligned}$$

where \mathcal{P} stands for the Cauchy principal value integral. In many cases, either the real or the imaginary part of $\chi(\omega)$ can be determined experimentally and the Kramers-Kronig transformation is used to obtain the entire complex response function. In the limit of $\omega=0$, these expressions are simplified to the following form, which shows close similarity with sum rules:

$$\Re\chi(\omega=0) \equiv \chi(0) = \frac{2}{\pi}\mathcal{P}\int_0^{\infty}\frac{\Im\chi(\omega)}{\omega}d\omega, \quad (1)$$

$$\Im\chi(\omega=0) \equiv 0 = -\frac{1}{\pi}\mathcal{P}\int_{-\infty}^{\infty}\frac{\Re\chi(\omega)}{\omega}d\omega. \quad (2)$$

Equation 1 shows that the static response of a system is fully determined by the corresponding dynamical susceptibility and the frequency denominator on the right-hand side indicates the vital role in low-energy excitations to the static susceptibility.

A common example is the dielectric permittivity of semiconductors, which is usually larger for compounds with smaller charge gap and can be considerably affected by the contributions from low-energy phonon modes. A particularly strong enhancement is found in quantum paraelectrics due to the presence of soft polar phonon modes.^{22,23} Besides low-energy or soft modes, in materials with ferroic orders, the ac susceptibility related to the domain dynamics can also influence the static response.

In multiferroic materials the coupling between the electric polarization and the magnetization can be phenomenologically described by the magnetoelectric susceptibility tensors $\chi^{me}(\omega)$ and $\chi^{em}(\omega)$, where $\Delta M_\gamma^\omega = \chi_{\gamma\delta}^{me}(\omega)E_\delta^\omega$ is the magnetization generated by an oscillating electric field and $\Delta P_\delta^\omega = \chi_{\delta\gamma}^{em}(\omega)H_\gamma^\omega$ is the polarization induced by an oscillating magnetic field, respectively. Here γ and δ stand for the Cartesian coordinates and the two cross-coupling tensors are connected by the $\{\dots\}'$ time-reversal operation according to $\{\chi_{\gamma\delta}^{me}(\omega)\}' = -\chi_{\delta\gamma}^{em}(\omega)$.

In a broad class of materials lacking simultaneously spatial inversion and time reversal symmetries,^{24–28} including also multiferroic compounds, the time reversal odd part of the ME susceptibility can induce a difference in the complex refractive index of counter-propagating electromagnetic waves,

$$N^\pm(\omega) \approx \sqrt{\varepsilon_{\delta\delta}(\omega)\mu_{\gamma\gamma}(\omega)} \pm \frac{1}{2} [\chi_{\gamma\delta}^{me}(\omega) - \{\chi_{\gamma\delta}^{me}(\omega)\}']. \quad (3)$$

Here N^\pm stands for the refractive indices of waves propagating in opposite directions ($\pm \mathbf{k}$). The \mathbf{e}_δ and \mathbf{e}_γ unit vectors are parallel to the direction of the electric (\mathbf{E}^ω) and magnetic (\mathbf{H}^ω) fields of light, respectively, while $\varepsilon_{\delta\delta}(\omega)$ and $\mu_{\gamma\gamma}(\omega)$ are diagonal components of the complex relative permittivity and permeability tensors in the $\{\mathbf{e}_\delta, \mathbf{e}_\gamma, \mathbf{e}_\eta\} \parallel \mathbf{k}$ basis. From this point on we restrict our study to those cases, when the solutions of the Maxwell equations are linearly polarized waves or the linear polarization of the incident light is nearly preserved during the propagation through the magnetoelectric medium. This condition needs to be satisfied to have direct comparison between the static and optical ME data. The difference in the imaginary part of the N^+ and N^- refractive indices gives rise to a difference in the absorption coefficients of counter-propagating waves, termed as directional dichroism:

$$\Delta\alpha(\omega) = \alpha_+(\omega) - \alpha_-(\omega) = \frac{2\omega}{c} \Im(\chi_{\gamma\delta}^{me}(\omega) - \{\chi_{\gamma\delta}^{me}(\omega)\}'), \quad (4)$$

where c is the speed of light in vacuum.

II. RESULTS

A. The ME sum rule

In several classes of non-centrosymmetric magnets $\chi_{\gamma\delta}^{me}(\omega)$ is antisymmetric with respect to the time reversal, as listed

in Table I and discussed later in this article. In this case, the static ME properties and the optical directional dichroism are described by the same element of the ME tensor, hence, Eqs. 1 and 4 yield the following ME sum rule:

$$\chi_{\gamma\delta}^{me}(0) = \frac{c}{2\pi} \mathcal{P} \int_0^\infty \frac{\Delta\alpha(\omega)}{\omega^2} d\omega. \quad (5)$$

According to this sum rule the static ME effect is mostly governed by the directional dichroism of low-energy excitations, since the absorption difference, $\Delta\alpha$, is cut off by the ω^2 denominator at higher frequencies. The ME sum rule in Eq. 5 can also be derived using the Kubo formula as described in the Appendix.

Following Neumann's principle, we specify the symmetry of those magnetic crystals for which $\chi_{\gamma\delta}^{me}(\omega)$ changes sign upon the time reversal. This off-diagonal ME tensor component is antisymmetric if and only if

- (1) all spatial symmetry operations of the magnetic point group (MPG) transforming $\chi_{\gamma\delta}^{me}(\omega)$ into $-\chi_{\gamma\delta}^{me}(\omega)$ are combined with the time reversal operation, and there is at least one such symmetry operation present in the MPG and
- (2) none of the spatial symmetry operations that leave $\chi_{\gamma\delta}^{me}(\omega)$ invariant are combined with time reversal and
- (3) symmetry elements connecting $\chi_{\gamma\delta}^{me}(\omega)$ to $\chi_{\delta\gamma}^{me}(\omega)$ or $-\{\chi_{\delta\gamma}^{me}(\omega)\}'$ and symmetry elements transforming $\chi_{\gamma\delta}^{me}(\omega)$ to $-\chi_{\delta\gamma}^{me}(\omega)$ or $\{\chi_{\delta\gamma}^{me}(\omega)\}'$ are not present in the MPG at the same time.

When light propagates along the principal axis of the crystal labeled as the z axis, the off-diagonal tensor component $\chi_{xy}^{me}(\omega)$ can generate directional dichroism, where x and y axis are perpendicular to the z axis. These three conditions are fulfilled for $\chi_{xy}^{me}(\omega)$ if the MPG meets all of the following criteria: i) it contains either an \bar{n}_z' or $2'_x$ symmetry operation where $n \in \{1, 2, 3, 6\}$, ii) the MPG does not have any element combined with time reversal besides the previous ones and $\bar{4}_z'$, and iii) the MPG does not contain any of the previously listed operations without a subsequent time reversal. Here subscripts stand for the axis of the n -fold proper (n) or improper (\bar{n}) rotations, primes ($'$) following spatial transformations indicate the time reversal operation.

For light propagation along the y axis perpendicular to the principal z axis, $\chi_{xz}^{me}(\omega)$ can generate directional dichroism. In this case, the conditions (1)–(3) specifying the requirements of $\chi_{xz}^{me}(\omega)$ being antisymmetric with respect to the time reversal are fulfilled if the MPG matches all of the following criteria: i) it contains at least one symmetry element from $\{\bar{1}', \bar{2}_x', 2_y', 2_z', \bar{3}_z', 6_z'\}$, ii) the MPG does not have any element combined with the time reversal besides the previous ones, and iii) the MPG does not contain 4_z , $\bar{4}_z$ or any of the previously listed operations without a subsequent time reversal.

The MPGs fulfilling these requirements are listed in Table I together with example materials. For MPGs marked by asterisks, the refractive index of the corresponding materials

TABLE I: Crystallographic magnetic point groups (MPG) hosting χ_{xy}^{me} and χ_{xz}^{me} ME tensor elements, which are antisymmetric with respect to the time reversal, listed in the second and fifth columns, respectively. Here z denotes the principal symmetry axis and MPG are labeled in the international notation. The subscripts of the symmetry operations show the axes of the n proper and \bar{n} improper rotations and the axes perpendicular to the m mirror planes. Subscript d denotes the diagonal direction between the x and y coordinate axes. Symmetry operations marked by prime (\prime) are combined with the time reversal. The χ_{xy}^{me} and χ_{xz}^{me} ME tensor elements correspond to light propagation along the z and y axes, respectively. For the MPG marked with asterisks in the third and sixth columns, the solutions of the Maxwell equations in the transverse-wave approximation are linearly polarized waves. The few remaining MPG are chiral, hence, they show circular dichroism. Several example materials are given in the fourth and seventh columns, where H_α –if specified– stands for an external magnetic field pointing to the α crystallographic direction. In these cases x and z are the actual high-symmetry axes, i.e. for $H_{[100]}$, $H_{[001]}$ and $H_{[110]}$ the corresponding coordinates are x , z and again x , respectively. In hexagonal manganites ScMnO_3 and LuMnO_3 , there are coexisting magnetic phases with sample dependent temperature ranges,²⁹ thus, they are indicated in two lines of the table.

Crystal system	$\chi_{xy}^{me}(\omega) = -\{\chi_{xy}^{me}(\omega)\}'$		Materials	$\chi_{xz}^{me}(\omega) = -\{\chi_{xz}^{me}(\omega)\}'$		Materials
Triclinic	$\bar{1}_z$	*		$\bar{1}_z$	*	
Monoclinic	m'_z	*	$\text{Ni}_3\text{B}_7\text{O}_{13}\text{I}$; ³⁰ BiTeI $H_{[100]}$ ³¹	$2'_z$	*	LiCoPO_4 ; ³⁹ Cu_2OSeO_3 $H_{[110]}$; ⁴⁰ Co_3TeO_6 ^{41,a}
	$2_z m'_z$	*	TbOOH ; ³² $\text{Ba}_2\text{Ni}_3\text{F}_{10}$ ³³	$2'_z m_z$	*	TbPO_4 ; ⁴³ MnPS_3 ; ⁴⁴ Co_3TeO_6 17 K < T < 21 K ⁴¹
Rhombic	$m_x m_y m'_z$	*	LiNiPO_4 ^{34,b}	$m_x m_y 2'_z$	*	BCGO ; ¹⁰ SCSO ; ^{16,17} CCSO ; ¹² CuB_2O_4 ⁴⁵ $H_{[110]}$ ^c
				$2'_x 2_y 2'_z$	*	BCGO ; ¹¹ SCSO ; ^{16,17} CCSO ; ¹² CuB_2O_4 ⁵¹ $H_{[100]}$ ^d
Tetragonal	$4_z m'_z$	*	Nd_5Si_4 ³⁶			
	$2'_x m_d \bar{4}_z$	*				
	$2'_x 2'_d \bar{4}_z$	*				
	$m_x m_d \bar{4}_z m'_z$	*				
Rhombohedral	$\bar{3}_z$	*	Cr_2O_3 ³⁷	$\bar{3}_z$	*	Cr_2O_3 ³⁷
				$m'_y \bar{3}_z$	*	BiTeI $H_{[001]}$ ³¹
	$2'_x \bar{3}_z$	*	$\text{Gd}_2\text{Ti}_2\text{O}_7$ ³⁸	$2'_x \bar{3}_z$	*	$\text{Gd}_2\text{Ti}_2\text{O}_7$ ³⁸
	$m_x \bar{3}_z$	*		$m_x \bar{3}_z$	*	$\text{Nb}_2\text{Mn}_4\text{O}_9$, $\text{Nb}_2\text{Co}_4\text{O}_9$ ⁵³
				$m'_y \bar{3}_z$	*	ScMnO_3 , LuMnO_3 ²⁹
Hexagonal	$\bar{6}_z$	*		$\bar{6}_z$	*	
	$6_z m'_z$	*		$\bar{6}_z m_z$	*	
	$m_x 2'_y \bar{6}_z$	*		$2'_x m'_y \bar{6}_z$	*	Fe_2P ⁵⁴
	$2'_x 2'_y \bar{6}_z$	*		$m_x m'_y \bar{6}'_z$	*	HoMnO_3 ; ^{29,55} YMnO_3 , ErMnO_3 , YbMnO_3 ^{29,e}
	$m_x m_y \bar{6}_z m'_z$	*		$2_y \bar{6}'_z$	*	
				$m_x m'_y \bar{6}'_z m_z$	*	

^a $\text{NdFe}_3(\text{BO}_3)_4$ $H_{[010]}$ ⁴²

^bone-dimensional photonic crystal with four-layered unit cell³⁵

^c CdS ;⁴⁶ AlN , GaN , InN $H_{[100]}$;⁴⁷ $\text{CaBaCo}_4\text{O}_7$;⁴⁸ GaFeO_3 ;⁴⁹ $\text{Co}_3\text{B}_7\text{O}_{13}\text{Br}$;⁵⁰ KMnFeF_6 ³³

^d Cu_2OSeO_3 $H_{[100]}$;⁴⁰ $[\text{Ru}(\text{bpy})_2(\text{ppy})][\text{MnCr}(\text{ox})]$;⁵² one-dimensional photonic crystal with three-layered unit cell³⁵

^e ScMnO_3 , LuMnO_3 , TmMnO_3 ²⁹

is described by Eq. 3. In all these MPG, the solutions of the Maxwell-equations are linearly polarized waves. In some of these cases, when there is a finite magnetization perpendicular to the light propagation, the polarization can have a small longitudinal component, which is neglected here. This transverse-wave approximation means that we neglect additional terms in the refractive index, which are higher-order products of tensor components like $\chi_{yz}^{me} \epsilon_{zx} / \epsilon_{zz}$ or $\chi_{zy}^{me} \mu_{zx} / \mu_{zz}$ for propagation along the z axis.

In materials belonging to MPG not marked by asterisk, natural and magnetic circular dichroism can appear, since these MPG are all chiral and in some cases finite magnetization is allowed parallel to the light propagation direction (Faraday configuration). However, for sufficiently thin samples the linear polarization of the incident light is nearly pre-

served even then. Thus, the index of refraction can be approximated by Eq. 3 for all of the listed MPG. This allows a direct comparison between the static and dynamical ME effects according to the ME sum rule in Eq. 5, since the static measurements used to determine the off-diagonal ME tensor elements can be compared to the optical experiments with linearly polarized light. In the second and third rows of Fig. 1 the $2'_x 2_y 2'_z$ chiral state of BCGO ¹¹ and CCSO ¹² is studied in the Faraday configuration, where the material shows polarization rotation. Nevertheless, the directional dichroism can be well approximated by Eq. 4.¹¹

B. Application of the ME sum rule to multiferroic materials

In order to check the applicability of the ME sum rule, we compare the magnetic field dependence of the static and optical ME effects for three members of the multiferroic melilite family, namely for $\text{Ba}_2\text{CoGe}_2\text{O}_7$, $\text{Ca}_2\text{CoSi}_2\text{O}_7$ and $\text{Sr}_2\text{CoSi}_2\text{O}_7$. These compounds crystallize in the non-centrosymmetric tetragonal $\text{P4}_2\text{m}$ structure^{56–59} where Co^{2+} cations with $S=3/2$ spin form square-lattice layers stacked along the tetragonal [001] axis. They undergo an antiferromagnetic transition at $T_N \approx 6\text{--}7\text{ K}$. Due to strong single-ion anisotropy, the two-sublattice antiferromagnetic state has an easy-plane character with spins lying within the tetragonal plane.^{20,58,60–62} The free rotation of the magnetization within the tetragonal plane can already be realized by moderate fields of $\lesssim 1\text{--}2\text{ T}$, which is an indication of a weak in-plane anisotropy.^{18,63} As another consequence of the single-ion anisotropy, the magnetization is saturated at different magnetic field values, $H_{\text{plane}}^{\text{sat}}$ and $H_{\text{axis}}^{\text{sat}}$, when the field is applied within the easy plane and along the hard axis, respectively.

Prior to saturation, the magnetization follows a nearly linear field dependence due to the increasing canting of the sublattice moments for any direction of the magnetic field.

The multiferroic character of these materials has been intensively studied both theoretically,^{64–66} and experimentally^{16–20,60,67} via their static ME properties. The strong optical ME effect emerging at their spin-wave excitations has also attracted much interest.^{10–12,68–70,72} The magnetically induced ferroelectric polarization has been described by the spin-dependent hybridization of the Co^{2+} d orbitals with the p orbitals of the surrounding oxygen ions forming tetrahedral cages.^{18,19} When the magnetization is a linear function of the applied field, the direction of the sublattice magnetizations can be straightforwardly expressed as a function of the orientation and the magnitude of the magnetic field. Then, the components of the magnetically induced ferroelectric polarization are directly determined from the orientation of the sublattice magnetizations within the spin-dependent hybridization model:^{18,71}

$$P_{[100]} = A_{\text{plane}} \left[\frac{H \sin \theta}{H_{\text{plane}}^{\text{sat}}} - \sqrt{1 - \left(\frac{H \sin \theta}{H_{\text{plane}}^{\text{sat}}} \right)^2} \right] \sqrt{1 - \left(\frac{H \cos \theta}{H_{\text{axis}}^{\text{sat}}} \right)^2} \frac{H \cos \theta}{H_{\text{axis}}^{\text{sat}}} \sin \phi, \quad (6)$$

$$P_{[010]} = A_{\text{plane}} \left[\frac{H \sin \theta}{H_{\text{plane}}^{\text{sat}}} - \sqrt{1 - \left(\frac{H \sin \theta}{H_{\text{plane}}^{\text{sat}}} \right)^2} \right] \sqrt{1 - \left(\frac{H \cos \theta}{H_{\text{axis}}^{\text{sat}}} \right)^2} \frac{H \cos \theta}{H_{\text{axis}}^{\text{sat}}} \cos \phi, \quad (7)$$

$$P_{[001]} = A_{\text{axis}} \left[\left(\frac{H \sin \theta}{H_{\text{plane}}^{\text{sat}}} \right)^2 - \frac{H \sin \theta}{H_{\text{plane}}^{\text{sat}}} \sqrt{1 - \left(\frac{H \sin \theta}{H_{\text{plane}}^{\text{sat}}} \right)^2} - \frac{1}{2} \left[1 - \left(\frac{H \cos \theta}{H_{\text{axis}}^{\text{sat}}} \right)^2 \right] \right] \sin 2\phi. \quad (8)$$

Here θ and ϕ are the polar and azimuthal angles of the magnetic field relative to the [001] and [100] axes, respectively, and H is the magnitude of the field. A_{plane} and A_{axis} are constants describing the strength of the magnetoelectric coupling. To make the formulas more compact, the tilting angle of the two inequivalent oxygen tetrahedra in the unit cell was approximated by $\pi/4$, which is close to the experimental value of 48° for CCSO.²¹ For BCGO, the saturation fields are $H_{\text{plane}}^{\text{sat}} \approx 16\text{ T}$ and $H_{\text{axis}}^{\text{sat}} \approx 36\text{ T}$ as found both in the static⁶³ and optical experiments.⁷² By fitting the field dependence of the static polarization reproduced from Ref. 18,19 in Fig. 1(a) and (g), we obtain $A_{\text{plane}} = 410\text{ }\mu\text{C/m}^2$ and $A_{\text{axis}} = 180\text{ }\mu\text{C/m}^2$ for BCGO. Using these parameters, the field dependence of every component of the static $\chi_{\delta\gamma}^{\text{em}} = \partial P_\delta / \partial H_\gamma$ ME tensor can be calculated for BCGO according to Eqs. 6–8.

For these three compounds, several elements of the static ME tensor, which are used in the present study for comparison with the directional dichroism spectra, can be directly determined from the measured field dependence of the ferroelectric polarization reported in the literature. Only in those cases

when experimental curves are not available, the ME tensor elements are evaluated using the fitted parameters as described above.

Fig. 1(a) displays the ferroelectric polarization induced along the [001] axis in BCGO by magnetic fields applied parallel to the [110] direction, $P_{[001]}(H_{[110]})$, as reproduced from Ref. 18. The field dependence of the $\chi_{[001],[110]}^{\text{em}}$ static ME tensor element for external fields along the [110] axis, given by the derivative $\partial P_{[001]} / \partial H_{[110]}$, is shown in Fig. 1(c). Via the ME sum rule in Eq. 5, this element of the static ME tensor is related to the integral of the directional dichroism spectrum in the Voigt configuration, where the magnetic component of light is parallel to the static magnetic field applied along the [110] direction and the electric component of light is parallel to the [001] axis. In this configuration, the directional dichroism spectra reported for BCGO by Ref. 10 correspond to the difference of the red and blue curves in Fig. 1(b), which are the absorption spectra obtained for counter-propagating THz waves. The comparison between the static and optical data using Eq. 5 is shown Fig. 1(c).

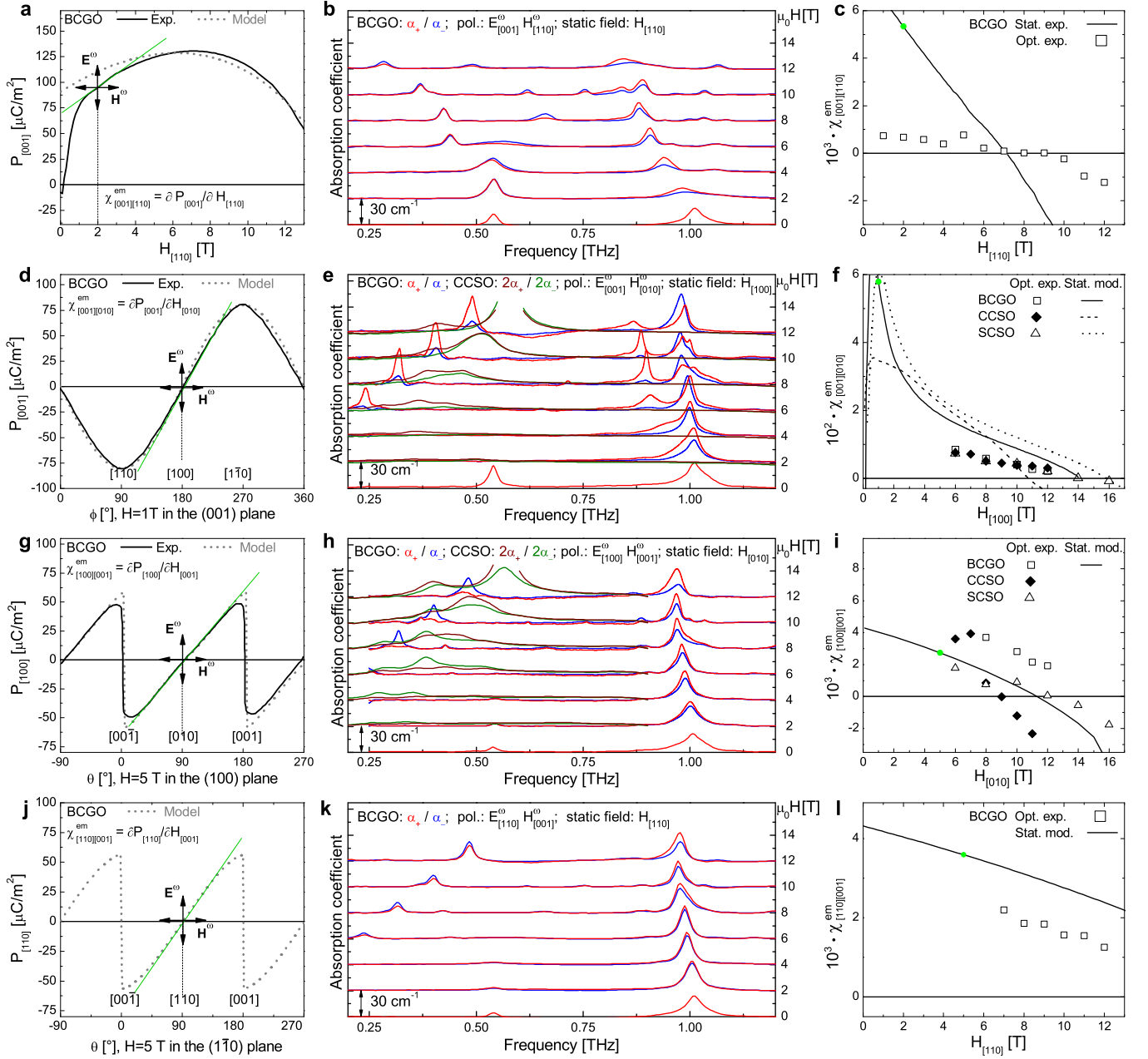


FIG. 1: (Color online) Comparison of the static and optical ME properties of multiferroic Ba₂CoGe₂O₇ (BCGO), Ca₂CoSi₂O₇ (CCSO) and Sr₂CoSi₂O₇ (SCSO) based on the ME sum rule in Eq. 5. Panel (a): Dependence of the ferroelectric polarization (P) on the magnitude of the magnetic field (H) in BCGO. Panels (d), (g) and (j): Dependence of P on the orientation of the field in BCGO. In these panels the solid lines are experimental data reproduced from Ref. 18, while the dashed lines are calculated using the spin dependent p-d hybridization model according to Eqs. 6-8.¹⁸ The slopes of the green lines in the same panels are proportional to the corresponding elements of the ME tensor. Arrows labeled with \mathbf{E}^ω and \mathbf{H}^ω show the electric and magnetic components of the absorbed light in the corresponding optical experiment, respectively. Panels (b), (e), (h) and (k): Field dependence of the magnon absorption spectra of BCGO in the GHz-THz range. The light polarizations indicated in these panels correspond to the labels \mathbf{E}^ω and \mathbf{H}^ω shown in the panels of the first column. The spectra are shifted vertically proportional to H . For BCGO, the spectra corresponding to counter-propagating light beams are plotted by red and blue lines, while for CCSO brown and dark green lines represent the two propagation directions. The absorption coefficient of CCSO is multiplied by a factor of two for better visibility. The spectra in panels (b) and (k) are measured in the present study, while the data in panels (e) and (h) are reproduced from Ref. 11 for BCGO and from Ref. 12 for CCSO, respectively. Panels (c), (f), (i) and (l): Magnetic field dependence of different components of the ME tensor. Symbols indicate the tensor elements calculated from the corresponding optical measurements using the ME sum rule; empty square, full diamond and empty triangle stand for BCGO, CCSO and SCSO, respectively. The field dependence of the static ME tensor components are plotted with solid, dashed and dotted lines for the three compounds in the same order. The points corresponding to the slope of the green lines in the left panels are indicated by a green dot. The solid line in panel (c) is calculated directly from the measured polarization-magnetic field curve shown on panel (a), while the curves in panels (f), (i) and (l) are evaluated using Eqs. 6-8. Static experiments, optical measurements and model calculations were carried out at $T=2$ K, $T=4$ K and $T=0$ K, respectively.

The following part of Fig. 1 shows similar analysis for other three elements of the ME tensor in BCGO. In two cases, data for SCSO and CCSO are also included. The dependence of the ferroelectric polarization on the orientation of a constant field H is shown in panels (d), (g) and (j). The directional dichroism spectra in these three cases are displayed in panels (e), (h) and (k), while the comparison between the static and optical data is given in panels (f), (i) and (l).

The $P_{[100]}(\theta)$ curve in Fig. 1(g) is reproduced from Ref. 18, where θ is the angle of the magnetic field relative to the $[001]$ axis. Since the tilting of the magnetic field from the $[010]$ direction by a small angle of $\delta\theta$ introduces a weak transversal field $\delta\mathbf{H}=(0, 0, H\sin\delta\theta)$, for $\mathbf{H}||[010]$ $\chi_{[100][001]}^{em}=\partial P_{[100]}/\partial H_{[001]}\approx 1/H\times\partial P_{[100]}/\partial\theta$. The corresponding optical experiment can be realized in the Faraday configuration, where $\mathbf{H}||[010]$, while the electric and magnetic components of light are parallel to the $[100]$ and $[001]$ axes, respectively. These THz absorption spectra are shown for the two opposite wave propagation directions in Fig. 1(h) as reproduced from Ref. 11 for BCGO and from Ref. 12 for CCSO.

The $P_{[001]}(\phi)$ curve in Fig. 1(d) is taken from Ref. 18 and the $P_{[110]}(\theta)$ curve in Fig. 1(j) is calculated using Eqs. 6-8. In the former and later cases, the elements of the static ME tensor are respectively obtained according to $\chi_{[001][010]}^{em}=P_{[001]}/\partial H_{[010]}\approx 1/H\times\partial P_{[001]}/\partial\phi$ for $\mathbf{H}||[100]$ and $\chi_{[110][001]}^{em}=P_{[110]}/\partial H_{[001]}\approx 1/H\times\partial P_{[110]}/\partial\theta$ for $\mathbf{H}||[110]$. The corresponding THz absorption spectra are shown in panels (e) and (k), respectively.

III. DISCUSSION

The comparison between the ME tensor elements calculated from the static and optical data in the last column of Fig. 1 supports the applicability of the ME sum rule in these multiferroic compounds. The magnitude and the field dependence of the static and optical data in panels (f), (i) and (l) show quantitative agreement. Their difference can be attributed to the following factors: i) the directional dichroism measurements were performed at $T=4$ K, while the static experiments were carried out at $T\leq 2$ K where the ME coefficients are larger by ~ 10 -20%, ii) the two set of experiments were performed on samples from different growths, iii) in Fig. 1(e) and (h) the polarization of light beams can change during the propagation through the samples due to natural and magnetic circular dichroism, iv) the model used to calculate the field dependence of the static ME coefficients is not accurate due to the linear field dependence of the magnetization assumed here to reduce the number of fitting parameters, and v) uncertainty in the geometrical factors of samples used in the static and optical experiments may also cause an error of typically ~ 10 -20%.

In the last three rows of Fig. 1 the dominant contribution to the integral in the ME sum rule comes from the Goldstone mode, whose excitation energy is proportional to the easy-plane component of the static magnetic field. This mode has a very small gap of less than 0.075 THz in zero field.⁷² In

the field region investigated here, its energy remains considerably smaller than those of the other magnon modes. Hence, it dominates the integral in the Eq. 5 sum rule due to the ω^2 frequency denominator. This mode is not allowed in an easy-plane magnet if the magnetic component of light is parallel to the static magnetic field as seen in Fig. 1(b). Correspondingly, in Fig. 1(c) the ME tensor element calculated from the directional dichroism data is smaller than those for the transverse spin excitations shown in panels (f), (i) and (l).

Moreover, the ME tensor element calculated from the sum rule in Fig. 1(c) is one order of magnitude smaller than the value determined from the static measurement, though they both change sign in the same field region of $\mu_0 H=7-9$ T. This significant difference may come from directional dichroism exhibited by excitations out of range of our optical detection. Since all magnon modes expected in the microscopic spin model of BCGO are observed in the absorption experiments,⁷² we think that low-energy phonon modes can show strong optical magnetoelectric effect due to coupling to magnon modes. Though directional dichroism has not been directly observed for phonon modes, recent optical studies on multiferroic $\text{Ba}_3\text{NbFe}_3\text{Si}_2\text{O}_{14}$ reported about the magnetoelectric nature of low-energy lattice vibrations.⁷³ As another possibility, spin excitations located out of our experimental window and not captured by the spin-wave theory can also contribute to the directional dichroism spectrum.

Besides the comparative analysis of static and optical ME data carried out for the three compounds above to demonstrate the applicability of the ME sum rule, we also make predictions for the same and other multiferroic materials. Previous studies report about magnetically induced ferroelectric polarization in the paramagnetic phase of BCGO¹⁹ and SCSO^{16,17} up to $T=300$ K, while their magnetic ordering temperature is $T_N\approx 7$ K. Since the magnetic symmetry (MPG) of these compounds depends on the orientation of the magnetic field but it is the same for the ordered and the paramagnetic state, we expect that the directional dichroism observed below T_N in various configurations can survive up to room temperature.

In the non-centrosymmetric soft magnet $(\text{Cu,Ni})\text{B}_2\text{O}_4$ the electric control of the magnetization direction has been demonstrated together with directional dichroism of near-infrared electronic excitations.⁷⁴ Since the contribution from these d-d transitions to the ME sum rule is negligible due to their high frequency and the ω^2 denominator in Eq. 5, we expect that directional dichroism should also be present for low-frequency magnon excitations in this material.

The magnetic control of the ferroelectric polarization and/or the electric control of the magnetization have been observed in a plethora of multiferroic materials including perovskite manganites with cycloidal spin order,⁷⁵⁻⁷⁸ the room temperature multiferroics BiFeO_3 ^{79,80} and $\text{Sr}_3\text{Co}_2\text{Fe}_{24}\text{O}_{41}$.^{81,82} Based on the ME sum rule, we predict that these compounds can also show directional dichroism as already has been found for $\text{Eu}_{0.55}\text{Y}_{0.45}\text{MnO}_3$ ¹³ and $\text{Gd}_{0.5}\text{Tb}_{0.5}\text{MnO}_3$ ¹⁴ in the spectral range of the magnon excitations.

IV. CONCLUSIONS

We derived a ME sum rule and discussed its validity for non-centrosymmetric magnets. We showed that the ME sum rule can be used to predict the static ME properties based on the directional dichroism spectra governed by the optical ME effect and vica versa, whenever the ME susceptibility of a material is antisymmetric with respect to the time reversal. We verified this approach by a quantitative comparison between static ME coefficients and directional dichroism spectra experimentally determined for three multiferroic compounds in the melilite family. In most cases we found that the dominant contribution to the ME sum rule comes from magnon excitations located in the GHz-THz region. Our approach is applicable to most of the magnetoelectric multiferroics, where the magnetically induced electric polarization can be controlled by the magnitude or the direction of external magnetic field.

We thank Y. Tokura, H. Murakawa and K. Penc for valuable discussions. This project was supported by Hungarian Research Funds OTKA K108918, TÁMOP-4.2.2.B-10/1-2010-0009, TÁMOP-4.2.1/B-09/1/KMR-2010-0002, TÁMOP 4.2.4. A/2-11-1-2012-0001, by the Estonian Ministry of Education and Research under Grants SF0690029s09 and IUT23-03, by the Estonian Science Foundation under Grants ETF8170 and ETF8703 and by the bilateral program of the Estonian and Hungarian Academies of Sciences under the Contract No. SNK-64/2013. S.B. was supported by the Funding Program for World-Leading Innovative R&D on Science and Technology (FIRST Program), Japan.

Appendix: Derivation of the magnetoelectric sum rule from the Kubo formula

The microscopic description of the linear response of a quantum system to external stimuli is given by the Kubo formula. For the frequency dependence of the ME susceptibility tensor, the finite-temperature Kubo formula reads

$$\chi_{\gamma\delta}^{me}(z) = -\frac{1}{\hbar} \sum_{m,n} \frac{e^{-\beta\hbar\omega_n} - e^{-\beta\hbar\omega_m}}{\sum_i e^{-\beta\hbar\omega_i}} \frac{\langle n | M_\gamma | m \rangle \langle m | P_\delta | n \rangle}{z - \omega_m + \omega_n}, \quad (\text{A.1})$$

where $z = \omega + i\varepsilon$ and $\varepsilon \rightarrow 0+$. M_γ and P_δ are the magnetic and electric dipole operators, respectively. $|m\rangle$ and $|n\rangle$ are eigenstates of the unperturbed system with energies of $\hbar\omega_m$ and $\hbar\omega_n$, while β is the inverse temperature. In the zero-temperature limit the Boltzmann factors vanish except for the $|0\rangle$ zero energy ground state:

$$\chi_{\gamma\delta}^{me}(z) = -\frac{1}{\hbar} \sum_m \left(\frac{\langle 0 | M_\gamma | m \rangle \langle m | P_\delta | 0 \rangle}{z - \omega_m} - \frac{\langle 0 | P_\delta | m \rangle \langle m | M_\gamma | 0 \rangle}{z + \omega_m} \right). \quad (\text{A.2})$$

If $\chi_{\gamma\delta}^{me}(\omega)$ is antisymmetric with respect to the time reversal, the $\langle 0 | M_\gamma | m \rangle \langle m | P_\delta | 0 \rangle$ product of the transition matrix elements of the magnetic and electric dipole operators is real. The imaginary part of the transition matrix element product vanishes since the magnetic dipole operator changes sign under time reversal operation, which also requires the conjugation of the matrix elements due to the exchange of the initial and final states. The Kubo formula at zero temperature for the real and imaginary part of the magnetoelectric susceptibility yields:

$$\Re \chi_{\gamma\delta}^{me}(\omega) = -\frac{2}{\hbar} \mathcal{P} \sum_m \frac{\omega_m \langle 0 | M_\gamma | m \rangle \langle m | P_\delta | 0 \rangle}{\omega^2 - \omega_m^2}, \quad (\text{A.3})$$

$$\Im \chi_{\gamma\delta}^{me}(\omega > 0) = \frac{\pi}{\hbar} \sum_m \langle 0 | M_\gamma | m \rangle \langle m | P_\delta | 0 \rangle \delta(\omega - \omega_m). \quad (\text{A.4})$$

These expressions can also be obtained by second order perturbation theory.⁸³ With $\Delta\alpha(\omega) = \frac{4\omega}{c} \Im \chi_{\gamma\delta}^{me}(\omega)$ one can reproduce Eq. 5:

$$\begin{aligned} \chi_{\gamma\delta}^{me}(0) &= \frac{2}{\hbar} \mathcal{P} \sum_m \frac{\langle 0 | M_\gamma | m \rangle \langle m | P_\delta | 0 \rangle}{\omega_m} \\ &= \frac{2}{\hbar} \mathcal{P} \sum_m \int_0^\infty \frac{\langle 0 | M_\gamma | m \rangle \langle m | P_\delta | 0 \rangle}{\omega} \cdot \delta(\omega - \omega_m) d\omega \\ &= \frac{c}{2\pi} \mathcal{P} \int_0^\infty \frac{\Delta\alpha(\omega)}{\omega^2} d\omega. \end{aligned} \quad (\text{A.5})$$

- ¹ A. J. Freeman and H. Schmid (eds.) *Magnetoelectric interaction phenomena in crystals* (Gordon and Breach, London, 1995).
- ² M. Fiebig, J. Phys. D: Appl. Phys. **38**, R123 (2005).
- ³ W. Eerenstein, N. D. Mathur and J. F. Scott, Nature **44**, 759 (2006).
- ⁴ R. Ramesh and N. A. Spaldin, Nat. Mater. **6**, 7 (2007).
- ⁵ L. W. Martin, Y.-H. Chuc and R. Ramesh, Materials Science and Engineering R **68**, 89 (2010).
- ⁶ S. M. Wu, Shane A. Cybart, D. Yi, James M. Parker, R. Ramesh and R. C. Dynes, Phys. Rev. Lett. **110**, 067202 (2013).
- ⁷ A. Pimenov, A. A. Mukhin, V. Y. Ivanov, V. D. Travkin, A. M. Balbashov and A. Loidl, Nat. Phys. **2** 97 (2006).
- ⁸ A. B. Sushkov, R. V. Aguilar, S. Park, S. W. Cheong and H. D.

- Drew, Phys. Rev. Lett., **98**, 027202 (2007).
- ⁹ P. Rovillain, R. De Sousa, Y. T. Gallais, A. Sacuto, M. A. Masson, D. Colson, A. Forget, M. Bibes, A. Barthélemy and M. Cazayous, Nat. Mater. **9**, 975 (2010).
- ¹⁰ I. Kézsmárki, N. Kida, H. Murakawa, S. Bordács, Y. Onose, and Y. Tokura, Phys. Rev. Lett. **106**, 057403 (2011).
- ¹¹ S. Bordács, I. Kézsmárki, D. Szaller, L. Demkó, N. Kida, H. Murakawa, Y. Onose, R. Shimano, T. Rõm, U. Nagel, S. Miyahara, N. Furukawa and Y. Tokura, Nat. Phys. **8**, 734 (2012).
- ¹² I. Kézsmárki, D. Szaller, S. Bordács, H. Murakawa, Y. Tokura, H. Engelkamp, T. Rõm, U. Nagel, arXiv:1310.0789 (2013).
- ¹³ Y. Takahashi, R. Shimano, Y. Kaneko, H. Murakawa and Y. Tokura, Nat. Phys. **8**, 121 (2012).

- ¹⁴ Y. Takahashi, Y. Yamasaki, and Y. Tokura, Phys. Rev. Lett. **111**, 037204(2013).
- ¹⁵ A. Shuvaev, V. Dziom, Anna Pimenov, M. Schiebl, A. A. Mukhin, A. C. Komarek, T. Finger, M. Braden, and A. Pimenov, Phys. Rev. Lett. **111** 227201 (2013).
- ¹⁶ M. Akaki, H. Iwamoto, T. Kihara, M. Tokunaga and H. Kuwahara, Phys. Rev. B **86**, 060413(R) (2012).
- ¹⁷ M. Akaki, T. Tadokoro, T. Kihara, M. Tokunaga and H. Kuwahara, J. Low Temp. Phys. **170**, 291 (2013).
- ¹⁸ H. Murakawa, Y. Onose, S. Miyahara, N. Furukawa and Y. Tokura, Phys. Rev. Lett. **105**, 137202 (2010).
- ¹⁹ H. Murakawa, Y. Onose, S. Miyahara, N. Furukawa, and Y. Tokura, Phys. Rev. B **85**, 174106 (2012).
- ²⁰ M. Akaki, J. Tozawa, D. Akahoshi and H. Kuwahara Appl. Phys. Lett. **94**, 212904 (2009).
- ²¹ K. Kusaka, K. Hagiya, M. Ohmasa, Y. Okano, M. Mukai, K. Iishi, N. Haga, Phys. Chem. Miner. **28**, 150 (2001).
- ²² Y. Yamada and G. Shirane, J. Phys. Soc. Jpn. **26**, 396 (1969).
- ²³ S. Kamba, D. Nuzhnyy, P. Vaněk, M. Savinov, K. Knížek, Z. Shen, E. Šantavá, K. Maca, M. Sadowski and J. Petzelt Europhys. Lett. **80** 27002 (2007).
- ²⁴ D. Szaller, S. Bordács and I. Kézsmárki, Phys. Rev. B **87**, 014421 (2013).
- ²⁵ R. M. Hornreich and S. Shtrikman, Phys. Rev. **171**, 1065 (1968).
- ²⁶ T. H. O'Dell, *The Electrodynamics of Magnetoelectric Media* (North-Holland, Amsterdam, 1970).
- ²⁷ T. Arima, J. Phys.: Condens. Matter. **20**, 434211 (2008).
- ²⁸ A. Cano, Phys. Rev. B **80**, 180416(R) (2009).
- ²⁹ M. Fiebig, Appl. Phys. B **74**, 749 (2002).
- ³⁰ J. P. Rivera and H. Schmid, Ferroelectrics **36**, 447 (1981).
- ³¹ A. V. Shevelkov, E. V. Dikarev, R. V. Shpanchenko, and B. A. Popovkin, J. Solid State Chem. **114**, 379 (1995).
- ³² D. E. Cox, Int. J. Magn. **6**, 67 (1974).
- ³³ G. Nénert and T. T. M. Palstra, J. Phys.: Condens. Matter **19**, 406213 (2007).
- ³⁴ R. P. Santoro, D. J. Segal, and R.E. Newnham, J. Phys. Chem. Solids **27**, 1192 (1966).
- ³⁵ A. Figotin, and I. Vitebsky, Phys. Rev. E **63**, 066609 (2001).
- ³⁶ J. M. Cadogan, D. H. Ryan, Z. Altounian, H. B. Wang, and I. P. Swainson, J. Phys. Condens. Matter **14**, 7191 (2002).
- ³⁷ J. Goulon, A. Rogalev, F. Wilhelm, C. Goulon-Ginet, P. Carra, D. Cabaret, and C. Brouder, Phys. Rev. Lett. **88**, 237401 (2002).
- ³⁸ J. R. Stewart, G. Ehlers, A. S. Wills, S. T. Bramwell, and J. S. Gardner, J. Phys. Condens. Matter **16**, L321 (2004).
- ³⁹ D. Vaknin, J. L. Zarestky, L. L. Miller, J.-P. Rivera, and H. Schmid, Phys. Rev. B **65**, 224414 (2002).
- ⁴⁰ S. Seki, S. Ishiwata, and Y. Tokura, Phys. Rev. B **86**, 060403(R) (2012).
- ⁴¹ P. Tolédano, V. Carolus, M. Hudl, T. Lottermoser, D. D. Khalyavin, S. A. Ivanov, and M. Fiebig, Phys. Rev. B **85**, 214439 (2012).
- ⁴² D. V. Volkov, A. A. Demidov, and N. P. Kolmakova, J. Exp. Theor. Phys. **104**, 897 (2007).
- ⁴³ S. Bluck, H. G. Kahle, J. Phys. C: Solid State Phys. **21**, 5193 (1988).
- ⁴⁴ E. Ressouche, M. Loire, V. Simonet, R. Ballou, A. Stunault, and A. Wildes, Phys. Rev. B **82**, 100408(R) (2010).
- ⁴⁵ M. Saito, K. Taniguchi, and T. Arima, J. Phys. Soc. Jpn. **77**, 013705 (2008).
- ⁴⁶ J. J. Hopfield and D. G. Thomas, Phys. Rev. Lett. **4**, 357 (1960).
- ⁴⁷ O. Ambacher, J. Phys. D: Appl. Phys. **31**, 2653 (1998).
- ⁴⁸ V. Caignaert, V. Pralong, V. Hardy, C. Ritter, and B. Raveau, Phys. Rev. B **81**, 094417 (2010).
- ⁴⁹ M. Kubota, T. Arima, Y. Kaneko, J. P. He, X. Z. Yu and Y. Tokura, Phys. Rev. Lett. **92**, 137401 (2004).
- ⁵⁰ M. E. Mendoza Alvarez, H. Schmid, and J. P. Rivera, Ferroelectrics **55**, 895 (1984).
- ⁵¹ M. Saito, K. Ishikawa, K. Taniguchi, and T. Arima, Phys. Rev. Lett. **101**, 117402 (2008).
- ⁵² F. Pointillart, M. Gruselle, G. André, and C. Train, J. Phys.: Condens. Matter **20**, 135214 (2008).
- ⁵³ A. Oleš, F. Kajzar, M. Kucab, and W. Sikora, *Magnetic Structures Determined by Neutron Diffraction* (Państwowe Wydawnictwo Naukowe, Warsaw, 1976).
- ⁵⁴ H. Fujii, Y. Uwatoko, K. Motoya, Y. Ito, and T. Okamoto, J. Phys. Soc. Jpn. **57**, 2143 (1988).
- ⁵⁵ M. Fiebig, C. Degenhardt, and R. V. Pisarev, J. Appl. Phys. **91**, 8867 (2002).
- ⁵⁶ K. Hagiya, M. Ohmasa and K. Iishi, Acta Cryst. **B49**, 172-179 (1993).
- ⁵⁷ Z. H. Jia, A. K. Schaper, W. Massa, W. Treutmann and H. Ragera, Acta Cryst. **B62**, 547555 (2006).
- ⁵⁸ A. Zheludev, T. Sato, T. Masuda, K. Uchinokura, G. Shirane and B. Roessli, Phys. Rev. B **68**, 024428 (2003).
- ⁵⁹ V. Hutanu, A. Sazonov, H. Murakawa, Y. Tokura, B. Náfrádi and D. Chernyshov, Phys. Rev. B **84**, 212101 (2011).
- ⁶⁰ M. Akaki, J. Tozawa, D. Akahoshi, and H. Kuwahara, J. Phys. C **150**, 042001 (2009).
- ⁶¹ T. Sato, T. Masuda, K. Uchinokura, Phys. B **329333**, 880 (2003).
- ⁶² V. Hutanu, A. Sazonov, M. Meven, H. Murakawa, Y. Tokura, S. Bordács, I. Kézsmárki, and B. Náfrádi, Phys. Rev. B **86**, 104401 (2012).
- ⁶³ A. P. Sazonov et al., to be published
- ⁶⁴ K. Yamauchi, P. Barone and S. Picozzi, Phys. Rev. B **84**, 165137 (2011).
- ⁶⁵ J.M., Perez-Mato, and J. L. Ribeiro, Acta Cryst. **A67**, 264268 (2011).
- ⁶⁶ P. Toledano, D. D. Khalyavin and L. C. Chapon, Phys. Rev. B **84**, 094421 (2011).
- ⁶⁷ H. T. Yi, Y.J. Choi, S. Lee and S. W. Cheong, Appl. Phys. Lett. **92**, 212904 (2008).
- ⁶⁸ S. Miyahara and N. Furukawa, J. Phys. Soc. Jpn. **80**, 073708 (2011).
- ⁶⁹ S. Miyahara and N. Furukawa, J. Phys. Soc. Jpn. **81**, 023712 (2012).
- ⁷⁰ M. Matsumoto, M. Soda, and T. Masuda, J. Phys. Soc. Jpn. **82**, 093703 (2013).
- ⁷¹ T. Arima J. Phys. Soc. Jpn. **76**, 073702 (2007).
- ⁷² K. Penc, J. Romhányi, T. Rődm, U. Nagel, Á. Antal, T. Fehér, A. Jánossy, H. Engelkamp, H. Murakawa, Y. Tokura, D. Szaller, S. Bordács and I. Kézsmárki, Phys. Rev. Lett. **108**, 257203 (2012).
- ⁷³ L. Chaix, S. de Brion, F. Lévy-Bertrand, V. Simonet, R. Ballou, B. Canals, P. Lejay, J. B. Brubach, G. Creff, F. Willaert, P. Roy, A. Cano, Phys. Rev. Lett. **110**, 157208 (2013).
- ⁷⁴ M. Saito, K. Ishikawa, S. Konno, K. Taniguchi and T. Arima, Nat. Mat. **8**, 634 (2009).
- ⁷⁵ Xiaoyan Yao and Qichang Li, Europhys. Lett. **88** 47002 (2009).
- ⁷⁶ Xiaoyan Yao, J. Phys. Soc. Jpn. **79**, 043801 (2010).
- ⁷⁷ T. Kimura, T. Goto, H. Shintani, K. Ishizaka, T. Arima and Y. Tokura, Nature **426**, 55 (2003).
- ⁷⁸ H. Murakawa, Y. Onose, F. Kagawa, S. Ishiwata, Y. Kaneko and Y. Tokura, Phys. Rev. Lett. **101**, 197207 (2008).
- ⁷⁹ T. Zhao, A. Scholl, F. Zavaliche, K. Lee, M. Barry, A. Doran, M. P. Cruz, Y. H. Chu, C. Ederer, N. A. Spaldin, R. R. Das, D. M. Kim, S. H. Baek, C. B. Eom and R. Ramesh, Nat. Mater. **5**, 823 (2006).
- ⁸⁰ Seoungsu Lee, W. Ratcliff, S. W. Cheong, V. Kiryukhin, Appl. Phys. Lett. **92**, 192906 (2008).

- ⁸¹ Y. Kitagawa, Y. Hiraoka, T. Honda, T. Ishikura, H. Nakamura and T. Kimura, *Nat. Mater.* **9**, 797 (2010).
- ⁸² S. H. Chun, Y. S. Chai, B-G. Jeon, H. J. Kim, Y. S. Oh, I. Kim, H. Kim, B. J. Jeon, S. Y. Haam, J-Y. Park, S. H Lee, J-H. Chung, J-H. Park and K. H. Kim, *Phys. Rev. Lett.* **108**, 177201 (2012).
- ⁸³ L. D. Barron, *Molecular Light Scattering and Optical Activity* (Cambridge University Press, Cambridge, 2004).